Carbon and nitrogen dynamics in the coastal Japan Sea inferred from 15 years of measurements of stable isotope ratios of *Calanus sinicus*

Ken-ichi Nakamura[1,2], Atsushi Nishimoto[3], Saori Yasui-Tamura[1,4], Yoichi Kogure[1], Misato Nakae[1], Naoki Iguchi[1], Haruyuki Morimoto[1], Taketoshi Kodama[5]

[1]Fisheries Resources Institute, Japan Fisheries Research and Education Agency, Niigata, 951-8121, Japan
[2]Present address: Kokusai Kogyo Co. Ltd., Tokyo, 102-0085, Japan
[3]Fisheries Technology Institute, Japan Fisheries Research and Education Agency, Yokohama, 236-8648, Japan
[4]Present address: Department of Ocean Sciences, Tokyo University of Marine Science and Technology, Tokyo, 108-8477, Japan
[5]Fisheries Resources Institute, Japan Fisheries Research and Education Agency, Yokohama, 236-8648, Japan

Correspondence to: Taketoshi Kodama (takekodama@affrc.go.jp)

Abstract. We hypothesized that the carbon and nitrogen stable isotope ratios ($\delta^{13}C$ and $\delta^{15}N$) of the copepod *Calanus sinicus* would record changes on the coastal environment of the Japan Sea. Therefore, we monitored these isotope ratios during the spring at four stations in the Japan Sea from 2006 to 2020 to identify the changes of carbon and nitrogen dynamics of this area. The $\delta^{13}C$ values ranged from −24.7‰ to −15.0‰ and decreased from the spring bloom (February/March) to the post-bloom (June/July). These variation was attributed to changes in both the physiology of *C. sinicus* and phytoplankton $\delta^{13}C$. The $\delta^{15}N$ values ranged from 2.8‰ to 8.8‰. This $\delta^{15}N$ value indicated *C. sinicus* is a secondary producer, and the tendency of the $\delta^{15}N$ values to increase from the bloom to post-bloom was attributable to an increase of the $\delta^{15}N$ of the phytoplankton. A generalized linear model (GLM) approach indicated that variations of $\delta^{13}C$ can be explained largely with sea surface temperature, sea surface chlorophyll *a* concentration, carbon: nitrogen ratio of *C. sinicus* and geographic difference. The residuals of $\delta^{13}C$ in the GLM was decreased with year (−0.035‰ year^{-1}), suggested that $\delta^{13}C$ in *C. sinicus* was decreasing. The GLM approach in $\delta^{15}N$ of *C. sinicus* indicated $\delta^{15}N$ varies with sex or growth stages in addition to the same environmental parameters with $\delta^{13}C$. The residuals of $\delta^{15}N$ in the GLM did not show a significant interannual trend. These results suggested that carbon dynamics would be changing in the coastal Japan Sea in these 15 years.

1 Introduction

Coastal ocean ecosystems are important for human activities and have been greatly changed as a result of those activities (Halpern et al., 2008; Doney, 2010). The Japan Sea (the Sea of Japan), which has been greatly impacted by human activities and global climate change, is considered to be an oceanic microcosm of the changing global ocean (Chen et al., 2017). Monotonic changes have been detected in the chemical environment of the coastal area of the Japan Sea as well as of the global ocean (Ishizu et al., 2019; Ono, 2021; Kodama et al., 2016). In the surface waters of the Japan Sea, pH and concentrations of phosphate and dissolved oxygen have been decreasing during the last few decades (Ishizu et al., 2019; Ono, 2021; Kodama et

al., 2016), whereas anthropogenic inputs of nitrogen from the atmosphere to the Japan Sea have been increasing (Kitayama et al., 2012).

Stable isotope ratios of carbon and nitrogen have been employed as tools to discern both elemental cycles and environmental changes in marine ecosystems (Ohman et al., 2012; Lorrain et al., 2020; Ren et al., 2017) as well as metrics of the trophic positions of organisms in ecosystems (Aita et al., 2011). During the 21st century, the ^{13}C:^{12}C carbon isotopic ratio of tuna has been rapidly decreasing as a linear function with time, and the rate of decrease has been faster than would be expected based on the Suess effect and the increase of anthropogenic carbon emissions (Gruber et al., 1999). It has thus been hypothesized that lower-trophic-level ecosystems have changed on a global scale (Lorrain et al., 2020). The input of anthropogenic nitrogen from the atmosphere to the ocean has been increasing (Duce et al., 2008), and in the marginal seas of East Asia, the ^{15}N:^{14}N nitrogen isotopic ratio of the organic matter bound in coral skeletons has decreased with the increase of anthropogenic nitrogen deposition (Ren et al., 2017).

In this study, we focused on *Calanus sinicus*, one of the dominant copepod species in the coastal waters of the western North Pacific (Uye, 2000), including the Japan Sea (Kodama et al., 2018a). Copepods of the genus *Calanus* are the major component of the macrozooplankton in shelf and coastal ecosystems outside the tropics, and they are the major source of nutrition for pelagic fish (Uye, 2000). Coastal areas of the Japan Sea are spawning and nursery grounds for Japanese sardine (*Sardinops melanosticta*), Japanese anchovy (*Engraulis japonicus*), and Pacific bluefin tuna (*Thunnus orientalis*) (Nishida et al., 2020; Furuichi et al., 2020; Ohshimo et al., 2017), and the larvae of these species prey on both the larval and adult stages of *C. sinicus* (Hirakawa et al., 1997; Hirakawa and Goto, 1996; Kodama et al., 2017a). *Calanus sinicus* therefore plays an important role as a major component of the second trophic level in the Japan Sea.

Studies of the long-term carbon and nitrogen dynamics in the Japan Sea (Ishizu et al., 2019; Ono, 2021; Kodama et al., 2016) have suggested that monotonic changes are likely to occur throughout the coastal ecosystem of the Japan Sea as the climate changes on a global scale. Besides, the muscle of small pelagic fish in the Japan Sea and the East China Sea from 1996 to 2019 shows that annual mean ^{13}C:^{12}C and ^{15}N:^{14}N are monotonically decreased 0.08‰ year^{-1} and 0.05‰ year^{-1}, respectively (Ohshimo et al., 2021). These suggested that it was decreasing that the stable isotope ratios of carbon and nitrogen in food of small pelagic fish in the Japan Sea. However, isotope values of neither zooplankton nor phytoplankton which were reflected the chemical environment of the Japan Sea have rarely been reported. The goal of this study was therefore to understand the long-term variations of isotope ratios in the coastal area of the Japan Sea through fifteen-years analysis of the carbon and nitrogen stable isotope ratios of *C. sinicus*.

2 Materials and methods

2.1 Onboard observations

Onboard observations were conducted from pre-bloom to post-bloom in 2006–2020 during cruises of the R/V *Mizuho-Maru*, R/V *Yoko-Maru* (Japan Fisheries Research and Education Agency), and R/V *Dai-Roku Kaiyo-Maru* (Kaiyo Engineering Co., Ltd.) in the territorial waters of Japan in the Japan Sea, a marginal sea of the western North Pacific (Fig. 1). Four stations for collection of stable isotope samples were chosen: in Toyama Bay (TB), Iida Bay (IB), north of the Noto Peninsula (NN), and Wakasa Bay (WB). These four stations are among 26 stations described in a previous study (Kodama et al., 2018a) that reported a clear west-east gradient of zooplankton community structure in this area during the month of May. Station (stn) TB was located near the mouths of two rivers (the Sho River and Oyabe River, Fig. 1), and stn WB was in an area of restricted circulation in Wakasa Bay. The cruises were conducted during four time intervals: 1) the end of February and/or the beginning of March (described as March), 2) the end of April, 3) the middle or end of May, and 4) the end of June or beginning of July (described as June) (Fig. 1c). The March cruise corresponded to the early stage of the spring phytoplankton bloom, the April cruise was during the late stage of the bloom, and the May and June cruises occurred during post-bloom conditions according to Kodama et al. (2018b). The observations after 2015 were conducted only in April and May (Fig. 1c).

Copepods for stable isotope analyses were collected by towing a Bongo net (500-μm mesh and 70-cm mouth diameter) obliquely at 0.5 m s^{-1} from a depth of 75 or from 10 m above the bottom to the surface at each station. Collected samples were frozen and preserved at ≤−20°C until sorting at an onshore laboratory. Vertical profiles of temperature, salinity, and chlorophyll *a* concentrations were measured by using a conductivity-temperature-depth (CTD) sensor (Seabird, SBE9plus or SBE19plus) with an *in vivo* chlorophyll fluorescence sensor from a depth of 200 m to the surface. Temperature and salinity of the sensors were calibrated by the manufacturer every year. The surface seawater was sampled with a bucket for measurement of sea surface temperature (SST), sea surface salinity (SSS), and sea surface chlorophyll *a* concentration (SSC). SST and SSS were measured with a calibrated mercury thermometer and a salinometer (Autosal, Guildline Instruments), respectively. For measurement of chlorophyll *a* concentrations, particles in 300 ml of water were collected on a glass fiber filter (GF/F, Whatman) and the pigments were extracted with *N,N*-dimethylformamide. The chlorophyll *a* concentrations were estimated based on the fluorescence of the extract, which was measured with a fluorometer (10-AU, Turner Designs) (Holm-Hansen et al., 1965). The chlorophyll fluorescence sensor was calibrated using these discrete samples during each cruise. Nutrient concentrations at the surface were measured during some cruises after 2015. The procedures used for the nutrient analyses have been described by Kodama et al. (2015). We collected and measured stable isotope ratio of particulate organic matter (>0.7 μm) in April of 2017 (at 0 m depth, $n = 6$) and May of 2019 (at 10 and 30 m depths, $n = 6$) nearby the *C. sinicus* sampling sites (Fig. 1b).

2.2 Stable isotope analyses

Ninety-four frozen-preserved Bongo net samples were thawed at room temperature. From every single thawed sample, *Calanus sinicus* (Copepoda; Calanoida) adults or copepodite stage V were sorted as quickly and much as possible to avoid alteration of their condition under the dissecting microscope. The 28 samples were divided into subsamples as copepodite stage V (C5), adult female (F) and adult male (M), and other 66 samples were not divided. The physiological processes of *C. sinicus* were different among the stages and sex (Zhou et al., 2016; Pu et al., 2004b; Pu et al., 2004a). At least five individuals are necessary for measurement of stable isotope ratio. When *C. sinicus* was present richly in one sample, we prepared several subsamples to evaluate the variability of the analysis. Therefore, a total of 267 samples were prepared for measurement of stable isotope ratio. The 267 samples were wrapped in a tin disk after dried at 60°C in a drying oven for 36–48 h. Table 1 provides details about the numbers of subsamples. We measured the stable isotope ratios of every subsample.

The carbon and nitrogen stable isotope ratios of the samples were measured with a stable isotope ratio mass spectrometer (IsoPrime100; Elementar) coupled with an elemental analyzer (vario MICRO cube; Elementar). Stable isotope ratios of carbon and nitrogen were calculated as the per mil (‰) deviations from the corresponding standards using the following equation:

$$\delta^{13}C_{bulk} \text{ or } \delta^{15}N_{bulk} = [(R_{sample} / R_{standard}) - 1] \times 1000 \quad (1)$$

where R is the $^{13}C/^{12}C$ or $^{15}N/^{14}N$ ratio. The standards for carbon and nitrogen were L-alanine, and the references were Pee Dee Belemnite and atmospheric N_2, respectively. The precisions of the analyses were within 0.2‰ for both $\delta^{13}C$ and $\delta^{15}N$. Based on the precision of analyses of L-alanine, the $\delta^{13}C$ and $\delta^{15}N$ values for each sample were rounded off to one decimal place. The amounts of carbon and nitrogen in each sample were also recorded, and the carbon: nitrogen ratio (C/N ratio) of *C. sinicus* was calculated. We did not conducted lipid extracted processes, and thus we calculated the lipid free $\delta^{13}C$ ($\delta^{13}C_{ex}$) based on the $\delta^{13}C_{bulk}$, C/N ratio and equation reported by Smyntek et al. (2007).

2.3 Statistical analyses

At first, we applied simple statistical analyses for identification of the spatial, monthly and stage (C5, F, M) difference of $\delta^{13}C_{bulk}$, $\delta^{13}C_{ex}$ and $\delta^{15}N_{bulk}$, and he relationships between the $\delta^{13}C_{bulk}$, $\delta^{13}C_{ex}$ and $\delta^{15}N_{bulk}$ of *C. sinicus* and environmental parameters (SST, SSC and SSS). We applied ANOVA (analysis of variance) with Tukey's test for identification the spatial and monthly difference. At some stations, we measured the $\delta^{13}C_{bulk}$ or $\delta^{15}N_{bulk}$ of multiple subsamples, and we did the statistical analyses without averaging data from the same station.

The relationships between the $\delta^{13}C_{bulk}$, $\delta^{13}C_{ex}$ and $\delta^{15}N_{bulk}$ of *C. sinicus* and environmental parameters (SST, SSC and SSS) were analyzed using general linear models (GLMs) with the linear link function in R software (R Core Team, 2020). The structures of the GLMs were based on concepts articulated by Kodama et al. (2021). The $\delta^{13}C$ and $\delta^{15}N$ errors were assumed to be normal distributions, and explanatory variables were expressed as linear functions in the GLMs, with the exception of SSC, which was log transformed. Two types of GLMs were applied as follows:

$$\delta X \sim poly(\text{SST}, 2) + poly(log\text{SSC}, 2) + poly(\text{SSS}, 2) + poly(\text{C/N}, 2) + f(\text{stn}) + f(\text{stage}) \quad (2)$$

where δX, stn, stage represent the target $\delta^{13}C_{bulk}$ or $\delta^{15}N_{bulk}$, station (WB, NN, IB and TB) and copepod stages (C5, F, M and mixed), respectively. The arguments of the *f* functions were categorical variables used to simulate nonlinear relationships. The second argument of the *poly* functions (i.e., 2) indicates that the first argument was incorporated into a quadratic expression in the model, i.e., dome-shaped responses were included in the models. We added "mixed" to the stage categories, which is for the subsamples undivided into stages or sex. We applied this GLM approach to $\delta^{13}C_{ex}$ but the results except C/N ratio were very similar to $\delta^{13}C_{bulk}$, and thus we did not show the results of $\delta^{13}C_{ex}$.

Equation (2) was intended to consider environmental and geographical effects, but not to take into consideration monthly and interannual variations of stable isotope ratio at every station. We could theoretically have evaluated monthly and interannual variations at every station using interaction terms such as *f*(month):*f*(year):*f*(stn) in Eq. (2), but when we included those interaction terms, the generalized variance inflation factors (GVIFs) became infinite. We evaluated monthly and interannual variations of stable isotope ratios using the residuals (observation − prediction) of Eq. (2) (described as residual $\delta^{13}C$ and residual $\delta^{15}N$). The trends of the residual $\delta^{13}C$ and residual $\delta^{15}N$ were expected to indicate the trend of $\delta^{13}C_{bulk}$ and $\delta^{15}N_{bulk}$ excluded the interannual trends of environmental parameters and geographical effects. The times of sample collection were to some extent opportunistic (Fig. 1C), and thus comparisons of simple mean values of $\delta^{13}C_{bulk}$ and $\delta^{15}N_{bulk}$ could be misleading if interannual variations were significant. We did not apply *f*(month) and *f*(year) for explanatory variables in Eq. (2) because they have collinearity with other environmental parameters. The explanatory variables in the final version of Eq. (2) were determined on the basis of values of GVIFs and Akaike information criteria (AICs). We required that the GVIFs of explanatory variables be less than 10, and the model with the smallest AIC was accepted as the final model.

The "ggpredict" function in the "ggeffects" package (Lüdecke, 2018) was used to visualize the effect of the explanatory variables on the $\delta^{13}C_{bulk}$ or $\delta^{15}N_{bulk}$ values. When the categorical variables (i.e., stage and station) remained in the least-AIC models, their values were fixed for purposes of calculating the predicted values. Note that we considered the nonlinear effects of environmental variables using generalized additive models (GAMs) instead of Eq. (2). However, the AIC values were not greatly improved in the GAMs. In this study, we have therefore reported only the GLM results. All the data and program code are in Digital Commons Data (Nakamura et al., 2021).

3 Results

3.1 Environmental variables

Sea surface temperature (SST) increased from March to June at every station (Fig. 2a). The SST at WB, the westernmost station, was the highest among the four stations on every cruise. The SST ranges were 8.8–23.1°C, 9.5–21.9°C, 9.3–23.2°C, and 10.1–23.4°C at stations TB, IB, NN, and WB, respectively. Sea surface salinity (SSS) was low at the TB station (Fig. 2b). The ranges of SSS were 28.6–34.5, 33.1–34.3, 33.1–34.6, and 33.1–34.6 at stations TB, IB, NN, and WB, respectively. SSS was highest in May at the other three stations. Variations of sea surface chlorophyll *a* (SSC) concentration at TB differed from

those at the other stations. SSC was higher at TB than at the other stations during every month. In addition, SSC at TB was higher in June than in May (Fig. 2c). The SSC values fell in the ranges 0.02–7.45, 0.08–5.46, 0.05–9.07, and 0.08–6.60 μg L^{-1} at TB, IB, NN, and WB, respectively.

The $\delta^{13}C$ of POM ranged from −27.3‰ to −22.5‰ (mean ± standard deviation: −24.8 ± 1.6‰), and from −24.9‰ to −23.0‰ (−23.7 ± 0.7‰) in April of 2017 and May of 2019, respectively. The $\delta^{15}N$ of POM ranged 3.1–5.1‰ (4.1 ± 0.7‰), and 2.5–4.3‰ (3.5 ± 0.7‰) in April of 2017 and May of 2019, respectively.

The mean ± standard deviation of C/N ratio in *C. sinicus* 5.5 ± 2.6 g g^{-1}. The ranges of C/N ratio in *C. sinicus* were from 3.4 to 19.2 g g^{-1}. The C/N ratio was significantly different among the stages (ANOVA, $p < 0.001$): the ratio was highest in C5 (copepodite stage V, mean ± sd: 7.9 ± 4.0 g g^{-1}, $n = 61$), and lowest in F (adult female, 4.6 ± 0.8 g g^{-1}, $n = 78$). The monthly variations were also significant (ANOVA, $p < 0.001$); the C/N ratio in all of the stages is highest in April (Fig. 3a).

3.2 Stable isotope ratios of C and N

The means ± standard deviations of all of the *C. sinicus* $\delta^{13}C_{bulk}$, $\delta^{13}C_{ex}$ and $\delta^{15}N_{bulk}$ values were −20.6 ± 1.8‰ (−24.7‰ to −15.0‰), −19.6 ± 1.9‰ (−24.8‰ to −14.7‰) and 6.9 ± 1.2‰ (2.8–8.8‰), respectively. Besides, $\delta^{13}C_{bulk}$, $\delta^{13}C_{ex}$ and $\delta^{15}N_{bulk}$ values of *C. sinicus* in April of 2017 were −21.6 ± 0.6‰, −18.2 ± 1.3‰, and 8.1 ± 0.6‰, respectively. Those in May of 2019 were −23.7 ± 0.1‰, −22.2 ± 0.1‰, and 6.7 ± 0.4‰, respectively. Significant monthly variations were observed for both $\delta^{13}C_{bulk}$, $\delta^{13}C_{ex}$ and $\delta^{15}N_{bulk}$ at every station (ANOVA, $p < 0.001$, Fig. 4). The highest $\delta^{13}C_{bulk}$ values were observed in March at all four stations (TB: −17.5 ± 2.1‰; IB: −18.7 ± 1.1‰; NN: 18.7 ± 0.9‰; and WB: −18.5 ± 1.1‰, Fig 4a). The monthly mean $\delta^{13}C_{bulk}$ values decreased from March to May at all four stations, although there was only one sample at WB in May (Fig. 4a). In June, monthly mean $\delta^{13}C_{bulk}$ values were similar to those in May, except at NN. The mean $\delta^{13}C_{bulk}$ at NN was significantly lower in May (−22.4 ± 2.2‰) than in June (−21.2 ± 1.3‰) (ANOVA with Tukey's HSD test, $p = 0.028$). The monthly mean values were significantly different among stations in April and March (ANOVA, $p < 0.006$). In all four months, the $\delta^{13}C_{bulk}$ at NN was the lowest among the four stations, and there were significant differences between the $\delta^{13}C_{bulk}$ values at WB and at NN in April and between those at TB and at NN in May (ANOVA with Tukey's HSD test, $p < 0.006$). Comparing the $\delta^{13}C_{bulk}$ in *C. sinicus* among the stages, that of C5 was significantly lower than those of F and M (Fig. 3b, Tukey's HSD test, $p < 0.001$).

The monthly and spatial variations of $\delta^{13}C_{ex}$ in *C. sinicus* were similar to those of $\delta^{13}C_{bulk}$. The highest $\delta^{13}C_{bulk}$ values were observed in March at all four stations, which was same with $\delta^{13}C_{bulk}$ (Fig. 4b). The monthly mean $\delta^{13}C_{ex}$ values decreased from March to May or June at all four stations (Fig. 4b). The difference from $\delta^{13}C_{bulk}$ was the relationship to the stages: the significant differences among the stages were not observed in $\delta^{13}C_{ex}$ (Fig. 3c, ANOVA, $p = 0.186$).

The lowest monthly mean $\delta^{15}N_{bulk}$ was observed in March at all four stations (TB: 5.1 ± 0.8‰; IB: 5.1 ± 1.4‰; NN: 5.6 ± 1.3‰; and WB: 4.5 ± 1.0‰). The $\delta^{15}N_{bulk}$ values were significantly elevated in April (TB: 7.4 ± 1.3‰; IB: 7.3 ± 0.5‰; NN: 7.5 ± 0.5‰; and WB: 7.0 ± 0.7‰), and they were stable from April to June (ANOVA with Tukey's HSD test, $p > 0.2$) at all

four stations (Fig. 4c). The differences of the monthly values among stations were significant during all four months (ANOVA, $p < 0.037$): monthly $\delta^{15}N_{bulk}$ values at NN were highest among the four stations in every month. In March, April, and June, the $\delta^{15}N_{bulk}$ values were significantly lower at WB than at NN (ANOVA with Tukey's HSD test, $p < 0.03$), but there were no significant differences between other pairs of stations. In May, the values were significantly lower at TB and IB than at NN (ANOVA with Tukey's HSD test, $p < 0.003$). Comparing the $\delta^{15}N_{bulk}$ in *C. sinicus* among the stages, that of C5 was significantly higher than those of F and M (Fig. 3d, Tukey's HSD test, $p < 0.017$), and those of F, M and mixed were the same level (Tukey's HSD test, $p > 0.8$).

3.3 Relationships between environmental parameters

There were significant linear relationships between the $\delta^{13}C_{bulk}$, $\delta^{13}C_{ex}$, and $\delta^{15}N_{bulk}$ values and SST, logarithm-transformed SSC, SSS and C:N ratio. The nature of the relationships was similar between $\delta^{13}C_{bulk}$ and $\delta^{13}C_{ex}$, but those differed between $\delta^{13}C_{bulk}$ and $\delta^{15}N_{bulk}$ (Fig. 5). The Pearson's correlation coefficient was negative between $\delta^{13}C_{bulk}$ or $\delta^{13}C_{ex}$ and SST ($p < 0.001$, Fig 5a, b), negative between $\delta^{13}C_{bulk}$ or $\delta^{13}C_{ex}$ and SSS ($p < 0.001$, Fig 5d, e) and positive between $\delta^{13}C_{bulk}$ or $\delta^{13}C_{ex}$ and logarithm-transformed SSC ($p < 0.001$, Fig 5g, h). In contrast, the Pearson's correlation coefficient was positive between $\delta^{15}N_{bulk}$ and both SST ($p < 0.001$, Fig 5c) and SSS ($p < 0.001$, Fig 5f), and it was negative between $\delta^{15}N_{bulk}$ and logarithm-transformed SSC ($p < 0.001$, Fig 5i). When an outlier value of SSS was removed (SSS was 28 in March at TB), the correlations with SSS were still significant. The C:N ratios of *C. sinicus* were negatively and positively correlated with $\delta^{13}C_{bulk}$ and $^{13}C_{ex}$, respectively (both $p < 0.001$, Fig. 5j, k). The C:N ratio was positively correlated with $\delta^{15}N_{bulk}$ ($p < 0.01$, Fig 5l).

In the least-AIC models with Eq. (2), SSS was removed from the full model in the cases of both $\delta^{13}C_{bulk}$ and $\delta^{15}N_{bulk}$. In addition, stage was not selected in the least-AIC model of $\delta^{13}C_{bulk}$. Thus, the following equations were the least-AIC models.

$$\delta^{13}C_{bulk} \sim -20.47\ (\pm 1.49) \times SST + 7.54\ (\pm 1.04) \times SST^2 + 2.82\ (\pm 1.54) \times log SSC + 0.70\ (\pm 1.16) \times (log SSC)^2 - 12.24\ (\pm 1.11) \times C/N + 8.13\ (\pm 1.04) \times C/N^2 + f(stn) \quad (3)$$

$$\delta^{15}N_{bulk} \sim 9.11\ (\pm 1.48) \times SST - 7.46\ (\pm 1.03) \times SST^2 + 0.26\ (\pm 1.43) \times log SSC - 2.39\ (\pm 1.12) \times (log SSC)^2 + 3.97\ (\pm 1.27) \times C/N - 0.46\ (\pm 1.05) \times C/N^2 + f(stn) + f(stage) \quad (4)$$

The coefficients of determination (r^2 values) of the least-AIC $\delta^{13}C$ and $\delta^{15}N$ models were 0.712 and 0.448, respectively. The effects of all variables were significant except *log*SSC in $\delta^{13}C_{bulk}$.

The least-AIC models produced convex graphs of $\delta^{13}C$ as a function of SST or C/N ratio (Fig. 6a, c). The minima of the $\delta^{13}C_{bulk}$ values occurred at approximately 20°C and 14 in the case of SST and the C/N ratio, respectively (Fig. 6a, c). Inter-station comparisons indicated that the $\delta^{13}C_{bulk}$ values were 0.6–1.1‰ higher at WB and TB than at IB and NN (Fig. 6d).

The responses of $\delta^{15}N_{bulk}$ to SST were the mirror image of the $\delta^{13}C_{bulk}$ responses to SST (Fig. 6e). The least-AIC model produced concave graph of $\delta^{15}N_{bulk}$ as a function of *log*SSC (Fig. 6f). The $\delta^{15}N_{bulk}$ maxima occurred at approximately 18°C and 1 μg L^{-1} in the case of SST and SSC (Fig. 6e, f). Inter-station comparisons indicated that $\delta^{15}N_{bulk}$ values were lowest at

WB and highest at NN (Fig. 6g). The comparison among the stages indicated that $\delta^{15}N_{bulk}$ values were lowest in F, and highest in C5 and mixed samples (Fig. 6h).

3.4 Temporal variations of residuals

The residual $\delta^{13}C$ [residuals of $\delta^{13}C_{bulk}$ based on GLM described by Eq. (3)] showed significant interannual variations (ANOVA, p <0.001, Fig. 7a), but no significant monthly variations (ANOVA, p = 0.09, Fig. 7b). Besides, the residual $\delta^{13}C$ showed that significant negative relationship between year (t-test, p = 0.0035, Fig. 7a). The coefficient (± standard error) of this relationship between residual $\delta^{13}C$ and year was −0.0365 ± 0.0124 ‰ year^{-1}. Calculating the relationships between residual $\delta^{13}C$ and year at every station, the significant negative relationships were only observed at stn. NN (t-test, p < 0.001). The high annual mean residual $\delta^{13}C$ values were observed in 2006 (mean ± standard deviation:0.51 ± 0.89‰), 2007 (0.72 ± 0.99‰), 2015 (0.44 ± 1.01‰) and 2020 (0.55 ± 0.11‰) (Fig. 7a).

Interannual variations of residual $\delta^{15}N$ [residuals of $\delta^{15}N_{bulk}$ based on GLM described by Eq. (4)] were also significant (ANOVA, p <0.001, Fig. 7c), but the linear trend was not significant (t-test, p = 0.053). The monthly variations of the residual $\delta^{15}N$ were significant (ANOVA, p <0.001), and increased significantly from March to April (Fig. 7d). The low annual mean residual $\delta^{15}N$ values were observed in 2012 (−0.59 ± 0.63‰), 2014(−0.80 ± 0.81‰) and 2020 (−0.97 ± 0.73‰) (Fig. 7a).

4. Discussion

Our aims of this study were to understand the long-term variations of isotope ratios in the coastal area of the Japan Sea, and thus we firstly discussed that the $\delta^{13}C_{bulk}$, $\delta^{13}C_{ex}$ and $\delta^{15}N_{bulk}$ of *C. sinicus* are reflected the $\delta^{13}C$ and $\delta^{15}N$ of POM, and then the dynamics of carbon and nitrogen. The *in situ* environment, however, is not immediately reflected in the $\delta^{13}C$ and $\delta^{15}N$ values of secondary producers. The turnover of carbon and nitrogen in copepod tissues must also be considered. Zooplankton production has not been reported in the Japanese coastal waters of the Japan Sea, but in the Kuroshio area, Kobari et al. (2018) have reported zooplankton production to be 0.7–1.0 mg C m^{-3} day^{-1} and zooplankton dry-weight (not carbon-weight) biomass to be 9.3–13.4 mg m^{-3}. If the carbon content of *C. sinicus* is half its dry weight (Omori, 1969), the reported production rate is approximately 15% of the *C. sinicus* biomass per day. If the metabolism of carbon is ignored, one week is necessary for turnover of the carbon of *C. sinicus*. This turnover time agrees with that of *Calanus finmarchicus*, 5–10 days (Mayor et al., 2011). This turnover time implies that monthly variations of the $\delta^{13}C$ and $\delta^{15}N$ of *C. sinicus* correspond to monthly variations of the environmental climatology.

The enrichment of $\delta^{15}N$ per tropic level is considered as 3.0 ± 1.0‰ (Aita et al., 2011). *Calanus sinicus* is the secondary producer that connect primary producers with higher trophic levels in the coastal area of the Japan Sea, although *C. sinicus* is known to prey on heterotrophic plankton in addition to phytoplankton (Hirai et al., 2018; Yi et al., 2017; Uye and Yamamoto, 1995). The mean $\delta^{15}N_{bulk}$ values of *C. sinicus* (6.9 ± 1.2‰) are consistent with this scenario: their $\delta^{15}N$ values are intermediate between those of particulate organic matter (POM) in coastal areas of the Japan Sea (around 2–6‰) (Kogure, 2004; Antonio

et al., 2012) and predatory fishes such as Japanese anchovy (8.9–11.7‰) (Tanaka et al., 2008) and Japanese sardines (9.4 ± 0.7‰) (Ohshimo et al., 2019). In particular, the differences of $\delta^{15}N$ between POM and *C. sinicus* were 4.0‰ and 3.2‰ in April 2017 and May 2019, respectively. These differences of $\delta^{15}N$ are within the ranges of nitrogen discrimination factor, 3.0 ± 1.0‰ (Aita et al., 2011). We found the $\delta^{15}N_{bulk}$ is different among the stages (Copepodite V, adult female, and male), and these suggested their preys or nitrogen metabolism are different among the stages, but the differences among the stages were small (≤0.5‰). Therefore, the case studies in April 2017 and May 2019 suggested that $\delta^{15}N_{bulk}$ of *C. sinicus* is reflected the $\delta^{15}N$ values of POM in the same month. Based on the monthly variations of $\delta^{15}N_{bulk}$, the $\delta^{15}N$ of the phytoplankton (POM) increases in the Japan Sea during the decline of the spring phytoplankton bloom. This is corresponding to seasonal variation of $\delta^{15}N$ of POM in the Kuroshio Current, which flows through Japanese coastal waters on the Pacific side of Japan: the $\delta^{15}N$ of POM increases from winter to spring because of Rayleigh fractionation as the inorganic nitrogen concentrations in the ambient water decrease (Kodama et al., 2021).

In contrast to $\delta^{15}N$, the relationship between $\delta^{13}C_{bulk}$ of *C. sinicus* and $\delta^{13}C$ of POM was different between April 2017 and May 2019: $\delta^{13}C_{bulk}$ of *C. sinicus* is 3.0‰ higher than $\delta^{13}C$ of POM in April 2017, but the difference was 0‰ in May 2019. At first, $\delta^{13}C_{bulk}$ were related with C/N ratio of *C. sinicus.* Therefore, the $\delta^{13}C_{bulk}$ values of *C. sinicus* during the bloom period was attributable to physiological changes of *C. sinicus*. *Calanus sinicus* is capable of storing oil in a sac (Zhou et al., 2016). The $\delta^{13}C$ values of copepods decrease with increases of their fatty acid content (Smyntek et al., 2007). This tendency was evidenced in this study by the relationship between the $\delta^{13}C_{bulk}$ values and C/N ratios of *C. sinicus*. The decline of $\delta^{13}C_{bulk}$ values with elevations of C/N ratio was therefore likely to have been the result of lipid accumulation in *C. sinicus.* The $\delta^{13}C_{ex}$ was more appreciate for identification of variations of carbon dynamics.

However, the relationship between $\delta^{13}C_{ex}$ of *C. sinicus* and $\delta^{13}C$ of POM was different between April 2017 (6.6‰) and May 2019 (1.5‰) as well as $\delta^{13}C_{bulk}$. The $\delta^{13}C$ of POM were not so different between April 2017 and May 2019, and the spatial variations were not so large as well. Therefore, considering turnover time of *C. sinicus* and spatiotemporal heterogeneity of $\delta^{13}C$ of POM, it was suggested that neither $\delta^{13}C_{bulk}$ nor $\delta^{13}C_{ex}$ of *C. sinicus* is not reflected the $\delta^{13}C$ of POM at the same station. Aita et al. (2011) reported that relationship between $\delta^{15}N$ and $\delta^{13}C$ in the marine plankton ecosystems are different among the seasons in the Oyashio area, western North Pacific, and the slopes of linear regression between $\delta^{15}N$ and $\delta^{13}C$ varies between 0.61 (in May) to 1.39 (in July). Therefore, variations of $\delta^{13}C_{bulk}$ and $\delta^{13}C_{ex}$ of *C. sinicus* were not only reflected the variations of $\delta^{13}C$ of POM, but also the carbon discrimination factor and metabolism of *C. sinicus.* The importance of carbon discrimination factor and metabolism of *C. sinicus* was observed in the monthly variation of $\delta^{13}C_{bulk}$ based on Eq. (3). In the present study, the monthly $\delta^{13}C$ of *C. sinicus* declined from the early stage to the late stage of the bloom or the post-bloom period. This trend has not been clearly apparent during seasonal monitoring of POM in the coastal area around Japan (Antonio et al., 2012; Kodama et al., 2021).

Neither the $\delta^{13}C_{bulk}$ nor $\delta^{13}C_{ex}$ were not reflected the $\delta^{13}C$ of POM, however, $\delta^{13}C_{bulk}$ was well explained ($r^2 = 0.712$) with the environmental parameters the GLM approach with Eq. (2). Besides, $\delta^{13}C_{bulk}$ was not different among the growth stages of copepod after adjustment by C/N ratio. Therefore, we considered that carbon discrimination factor and metabolism of *C.*

sinicus also vary with environmental parameters as well as $\delta^{13}C$ of POM. Therefore, the trends of residual $\delta^{13}C$ in Eq. (3) were considered as the trends of carbon dynamics unexplained with the environmental variables and metabolism of *C. sinicus*. The significant linear decreasing trend of residuals of $\delta^{13}C_{bulk}$ (-0.0365 ± 0.0124‰ year^{-1}) were observed in our study. This decreasing trend of $\delta^{13}C_{bulk}$ was slower than that decreasing trends of $\delta^{13}C$ values of tuna muscle, −0.12‰ year^{-1} (Lorrain et al., 2020), and the decreasing trend of $\delta^{13}C$ in small pelagic fish in the Japan Sea and East China Sea, −0.08‰ (Ohshimo et al., 2021). On the other hand, this decreasing trend of $\delta^{13}C_{bulk}$ was comparable to or slightly higher than the Suess effect which was reported as −0.025‰ year^{-1} (Gruber et al., 1999). These suggested that the decreasing trend of $\delta^{13}C$ in fish collected in the Japan Sea and East China Sea were supported by decreasing trends of $\delta^{13}C$ of their preys.

On the other hand, interannual linear trend of residual $\delta^{15}N$ were not significant. This is similar to some previous longer-term studies of zooplankton stable isotope ratios which have noted that the trends have not been strictly linear (Christensen and Richardson, 2008; Chiba et al., 2012), but different from the trend detected in small pelagic fish in the Japan Sea and East China Sea, −0.05‰ (Ohshimo et al., 2021). However, we could not conclude that the $\delta^{15}N$ of *C. sinicus* does not have a linear interannual trend, because the predicted $\delta^{15}N_{bulk}$ based on GLM contained some uncertainty based on our sampling design. The $\delta^{15}N_{bulk}$ was different among the stages and sex after applying the GLMs, and we did not evaluate the population structure of "mixed".

In this study, the decreasing trend of $\delta^{13}C_{bulk}$ was detected, however, this decline trends in the residuals of $\delta^{13}C_{bulk}$ was not homogenous when we calculated them at every station. In addition, the significant geographical differences were observed in both $\delta^{13}C_{bulk}$ and $\delta^{15}N_{bulk}$ values. Besides, not only straight linear trend, but also occasional elevations of residuals of $\delta^{13}C_{bulk}$ (2015 and 2020) and decline of residuals of $\delta^{15}N_{bulk}$ (2020) were observed. Some studies reported that eventual phenomena in the Japan Sea. For example, much nitrate was discharged by the Changjiang River into the Japan Sea during the summer of 2013 (Kodama et al., 2017b), and lowering of surface salinity by inflow from the Changjiang River occurred in the summer or autumn of 2010, 2012, and 2015 (Kosugi et al., 2021). However, we could not find any relationship between the occasional change of stable isotope ratios of *C. sinicus* and the reported eventual phenomena in the Japan Sea. We cannot clarify the causes of these occasional interannual variations. Our observations were opportunistic, and the measured environmental parameters were not sufficient for identifying these variations. Thus, we did not have any evidence, but some more local phenomena may be important. For example, $\delta^{15}N$ values of riverine nitrate differ as a function of their source: fertilizer, sewage, or forest soil, and their contributions are not stable (Sugimoto et al., 2019). These differences must impact to $\delta^{15}N$ values of marine ecosystems.

Conclusions

We used data of a 15-year study of the $\delta^{13}C_{bulk}$ and $\delta^{15}N_{bulk}$ of the calanoid copepod *C. sinicus* to indirectly examine long-term variations of stable carbon and nitrogen isotope ratios. The $\delta^{15}N_{bulk}$ indicated that *C. sinicus* was a "secondary" producer in the area. $\delta^{13}C_{bulk}$ of *C. sinicus* was reflected to not only $\delta^{13}C$ of phytoplankton, but also the physiological processes of *C. sinicus*,

but the variations of $\delta^{13}C_{bulk}$ were largely explained with environmental parameters, the geographical position and element ratio of *C. sinicus* using the GLM approach. $\delta^{15}N_{bulk}$ of *C. sinicus* was largely depended on $\delta^{15}N$ of phytoplankton, but difference of growth stage or sex were also affected to $\delta^{15}N_{bulk}$ of *C. sinicus*. The residuals between observed stable isotope ratios and GLM-predicted stable isotope ratios (residual $\delta^{13}C$ and residual $\delta^{15}N$) indicated that the residual $\delta^{13}C$ shows a significant linear decreasing trend, but the residual $\delta^{15}N$ did not show. The decreasing trend of residual $\delta^{13}C$ was -0.0365 ± 0.0124‰ year^{-1} is gentler than that observed in the muscle of small pelagic fish in the East China Sea and the Japan Sea, but comparable to the Suess effect. In addition to the decreasing trend, the occasional elevations of residual $\delta^{13}C$ and decline of residual $\delta^{15}N$ were observed. These occasional variations, however, were not coupled with a documented events in the Japan Sea. Therefore, we also concluded that undocumented, local-scale events also accounted for the changes of carbon and nitrogen dynamics in the coastal areas.

The linear decline trend of $\delta^{13}C$ in *C. sinicus* was detected in our 15 years observations, but it was not denied that this trend is one of phases of over-decadal variations. For example, the biomass of Japanese sardine, *Sardinops melanostictus*, shows several-decades variations in the Japan Sea (Kodama et al., 2018b). We need, therefore, more longer-term monitoring of stable isotope ratios to identify the variations. In addition, the trends of stable isotope ratios of *C. sinicus* were possibley different among the sampling sites. This spatial heterogeneity is a very important contributor to the high value of the ecosystem services provided by coastal areas, including their role as nursery grounds for many commercially valuable fish. Management of watersheds must be carried out at a local scale, and recruitment to local fisheries resources is sensitive to local disturbances. Global-scale and regional-scale environmental changes are very important, but local-scale changes are also important. More comparative studies that address local-scale effects are needed.

Code and Data availability

Our code and data are in Mendeley Data (http://dx.doi.org/10.17632/4z7vkn22tr.2).

Author contribution

KN, NI, HM and TK designed the experiments, KN, AN, SY, YK, MN, NI, HM and TK carried them out. KN, AN and TK prepared the manuscript with contributions from all co-authors.

Competing interests:

The authors declare that they have no conflict of interest.

Acknowledgements

Onboard observations were conducted through RVs *Mizuho-Maru* and *Yoko-Maru* of the Japan Fisheries Research and Education Agency and *Dai-Roku Kaiyo-maru* of Kaiyo Engineering Co. Ltd. We appreciate captains, crews, researchers, and staffs supporting us and participating in sampling in the cruises. We also thank K. Yamada and K. Matsuda for supports of onshore experiments. The funding is provided from Fisheries Agency of Japan, Japan Fisheries Research and Education Agency to all and JSPS KAKENHI (Grant-in-Aid for Scientific Research C No. 16K07831 and 19K06198) to TK and YK. The English in this manuscript was carefully corrected by two professional editors of ELSS, both with extensive research editing experience. One of these editors is a native English speaker.

References

Aita, M. N., Tadokoro, K., Ogawa, N. O., Hyodo, F., Ishii, R., Smith, S. L., Saino, T., Kishi, M. J., Saitoh, S.-I., and Wada, E.: Linear relationship between carbon and nitrogen isotope ratios along simple food chains in marine environments, J. Plankton Res., 33, 1629-1642, https://doi.org/10.1093/plankt/fbr070, 2011.

Antonio, E. S., Kasai, A., Ueno, M., Ishihi, Y., Yokoyama, H., and Yamashita, Y.: Spatial-temporal feeding dynamics of benthic communities in an estuary-marine gradient, Estuar. Coast. Shelf. Sci., 112, 86-97, https://doi.org/10.1016/j.ecss.2011.11.017, 2012.

Chen, C.-T. A., Lui, H.-K., Hsieh, C.-H., Yanagi, T., Kosugi, N., Ishii, M., and Gong, G.-C.: Deep oceans may acidify faster than anticipated due to global warming, Nat. Clim. Change, 7, 890-894, https://doi.org/10.1038/s41558-017-0003-y, 2017.

Chiba, S., Sugisaki, H., Kuwata, A., Tadokoro, K., Kobari, T., Yamaguchi, A., and Mackas, D. L.: Pan-North Pacific comparison of long-term variation in Neocalanus copepods based on stable isotope analysis, Prog. Oceanogr., 97-100, 63-75, https://doi.org/10.1016/j.pocean.2011.11.007, 2012.

Christensen, J. T. and Richardson, K.: Stable isotope evidence of long-term changes in the North Sea food web structure, Mar. Ecol. Prog. Ser., 368, 1-8, https://doi.org/10.3354/meps07635, 2008.

Doney, S. C.: The growing human footprint on coastal and open-ocean biogeochemistry, Science, 328, 1512-1516, https://doi.org/10.1126/science.1185198, 2010.

Duce, R. A., LaRoche, J., Altieri, K., Arrigo, K. R., Baker, A. R., Capone, D. G., Cornell, S., Dentener, F., Galloway, J., Ganeshram, R. S., Geider, R. J., Jickells, T., Kuypers, M. M., Langlois, R., Liss, P. S., Liu, S. M., Middelburg, J. J., Moore, C. M., Nickovic, S., Oschlies, A., Pedersen, T., Prospero, J., Schlitzer, R., Seitzinger, S., Sorensen, L. L., Uematsu, M., Ulloa, O., Voss, M., Ward, B., and Zamora, L.: Impacts of atmospheric anthropogenic nitrogen on the open ocean, Science, 320, 893-897, https://doi.org/10.1126/science.1150369, 2008.

Furuichi, S., Yasuda, T., Kurota, H., Yoda, M., Suzuki, K., Takahashi, M., and Fukuwaka, M.: Disentangling the effects of climate and density-dependent factors on spatiotemporal dynamics of Japanese sardine spawning, Mar. Ecol. Prog. Ser., 633, 157-168, 2020.

Gruber, N., Keeling, C. D., Bacastow, R. B., Guenther, P. R., Lueker, T. J., Wahlen, M., Meijer, H. A. J., Mook, W. G., and Stocker, T. F.: Spatiotemporal patterns of carbon-13 in the global surface oceans and the oceanic suess effect, Global Biogeochem. Cycles, 13, 307-335, https://doi.org/10.1029/1999gb900019, 1999.

Halpern, B. S., Walbridge, S., Selkoe, K. A., Kappel, C. V., Micheli, F., D'Agrosa, C., Bruno, J. F., Casey, K. S., Ebert, C., Fox, H. E., Fujita, R., Heinemann, D., Lenihan, H. S., Madin, E. M., Perry, M. T., Selig, E. R., Spalding, M., Steneck, R., and Watson, R.: A global map of human impact on marine ecosystems, Science, 319, 948-952, https://doi.org/10.1126/science.1149345, 2008.

Hirai, J., Hamamoto, Y., Honda, D., and Hidaka, K.: Possible aplanochytrid (Labyrinthulea) prey detected using 18S metagenetic diet analysis in the key copepod species *Calanus sinicus* in the coastal waters of the subtropical western North Pacific, Plank. Benth. Res., 13, 75-82, https://doi.org/10.3800/pbr.13.75, 2018.

Hirakawa, K. and Goto, T.: Diet of larval sardine, *Sardinops melanostictus* in Toyama Bay, southen Japan Sea, Bull. Japan Sea Reg. Fish. Res. Lab., 46, 65-75, 1996.
Hirakawa, K., Goto, T., and Hirai, M.: Diet composition and prey size of larval anchovy, *Eugraulis japonicus*, in Toyama Bay, Southern Japan Sea, Bull. Japan Sea Reg. Fish. Res. Lab., 47, 67-78, 1997.
Holm-Hansen, O., Lorenzen, C. J., Holmes, R. W., and Strickland, J. D.: Fluorometric determination of chlorophyll, Journal du Conseil, 30, 3-15, 1965.
Ishizu, M., Miyazawa, Y., Tsunoda, T., and Ono, T.: Long-term trends in pH in Japanese coastal seawater, Biogeosciences, 16, 4747-4763, https://doi.org/10.5194/bg-16-4747-2019, 2019.
Kitayama, K., Seto, S., Sato, M., and Hara, H.: Increases of wet deposition at remote sites in Japan from 1991 to 2009, Journal of Atmospheric Chemistry, 69, 33-46, https://doi.org/10.1007/s10874-012-9228-3, 2012.
Kobari, T., Makihara, W., Kawafuchi, T., Sato, K., and Kume, G.: Geographic variability in taxonomic composition, standing stock, and productivity of the mesozooplankton community around the Kuroshio Current in the East China Sea, Fish. Oceanogr., 27, 336-350, https://doi.org/10.1111/fog.12256, 2018.
Kodama, T., Igeta, Y., Kuga, M., and Abe, S.: Long-term decrease in phosphate concentrations in the surface layer of the southern Japan Sea, J. Geophys. Res., 121, 7845-7856, https://doi.org/10.1002/2016jc012168, 2016.
Kodama, T., Morimoto, H., Igeta, Y., and Ichikawa, T.: Macroscale-wide nutrient inversions in the subsurface layer of the Japan Sea during summer, J. Geophys. Res., 120, 7476-7492, https://doi.org/10.1002/2015jc010845, 2015.
Kodama, T., Nishimoto, A., Horii, S., Ito, D., Yamaguchi, T., Hidaka, K., Setou, T., and Ono, T.: Spatial and seasonal variations of stable isotope ratios of particulate organic carbon and nitrogen in the surface water of the Kuroshio, J. Geophys. Res., 126, e2021JC017175, https://doi.org/10.1029/2021jc017175, 2021.
Kodama, T., Wagawa, T., Iguchi, N., Takada, Y., Takahashi, T., Fukudome, K.-I., Morimoto, H., and Goto, T.: Spatial variations in zooplankton community structure along the Japanese coastline in the Japan Sea: influence of the coastal current, Ocean Sci., 14, 355-369, https://doi.org/10.5194/os-14-355-2018, 2018a.
Kodama, T., Hirai, J., Tamura, S., Takahashi, T., Tanaka, Y., Ishihara, T., Tawa, A., Morimoto, H., and Ohshimo, S.: Diet composition and feeding habits of larval Pacific bluefin tuna *Thunnus orientalis* in the Sea of Japan: integrated morphological and metagenetic analysis, Mar. Ecol. Prog. Ser., 583, 211-226, https://doi.org/10.3354/meps12341, 2017a.
Kodama, T., Morimoto, A., Takikawa, T., Ito, M., Igeta, Y., Abe, S., Fukudome, K., Honda, N., and Katoh, O.: Presence of high nitrate to phosphate ratio subsurface water in the Tsushima Strait during summer, J. Oceanogr., 73, 759-769, https://doi.org/10.1007/s10872-017-0430-4, 2017b.
Kodama, T., Wagawa, T., Ohshimo, S., Morimoto, H., Iguchi, N., Fukudome, K. I., Goto, T., Takahashi, M., and Yasuda, T.: Improvement in recruitment of Japanese sardine with delays of the spring phytoplankton bloom in the Sea of Japan, Fish. Oceanogr., 27, 289-301, https://doi.org/10.1111/fog.12252, 2018b.
Kogure, Y.: Stable carbon and nitrogen isotope analysis of the sublittoral benthic food web structure of an exposed sandy beach, Bull. Biogeogr. Soc. Jpn., 59, 15-25, 2004.
Kosugi, N., Hirose, N., Toyoda, T., and Ishii, M.: Rapid freshening of Japan Sea Intermediate Water in the 2010s, J. Oceanogr., 77, 269-281, https://doi.org/10.1007/s10872-020-00570-6, 2021.
Lorrain, A., Pethybridge, H., Cassar, N., Receveur, A., Allain, V., Bodin, N., Bopp, L., Choy, C. A., Duffy, L., Fry, B., Goni, N., Graham, B. S., Hobday, A. J., Logan, J. M., Menard, F., Menkes, C. E., Olson, R. J., Pagendam, D. E., Point, D., Revill, A. T., Somes, C. J., and Young, J. W.: Trends in tuna carbon isotopes suggest global changes in pelagic phytoplankton communities, Global Change Biolology, 26, 458-470, https://doi.org/10.1111/gcb.14858, 2020.
Lüdecke, D.: ggeffects: Tidy Data Frames of Marginal Effects from Regression Models, Journal of Open Source Software, 3, 772, https://doi.org/10.21105/joss.00772, 2018.
Mayor, D. J., Cook, K., Thornton, B., Walsham, P., Witte, U. F. M., Zuur, A. F., and Anderson, T. R.: Absorption efficiencies and basal turnover of C, N and fatty acids in a marine Calanoid copepod, Funct. Ecol., 25, 509-518, https://doi.org/10.1111/j.1365-2435.2010.01791.x, 2011.
Nakamura, K.-i., Nishimoto, A., Yasui-Tamura, S., Kogure, Y., Nakae, M., Iguchi, N., Morimoto, H., and Kodama, T.: Data for: Stable isotope ratio of *Calanus sinicus* in the coastal Japan Sea" (V2) [dataset], https://doi.org/10.17632/4z7vkn22tr.2, 2021.

Nishida, K., Yasu, A., Nanjo, N., Takahashi, M., Kitajima, S., and Ishimura, T.: Microscale stable carbon and oxygen isotope measurement of individual otoliths of larvae and juveniles of Japanese anchovy and sardine, Estuar. Coast. Shelf. Sci., 245, 106946, https://doi.org/10.1016/j.ecss.2020.106946, 2020.

Ohman, M. D., Rau, G. H., and Hull, P. M.: Multi-decadal variations in stable N isotopes of California Current zooplankton, Deep Sea Res. I, 60, 46-55, https://doi.org/10.1016/j.dsr.2011.11.003, 2012.

Ohshimo, S., Kodama, T., Yasuda, T., Kitajima, S., Tsuji, T., Kidokoro, H., and Tanaka, H.: Potential fluctuation of δ13C and δ15N values of small pelagic forage fish in the Sea of Japan and East China Sea, Mar. Freshwater Res., https://doi.org/10.1071/mf20351, 2021.

Ohshimo, S., Madigan, D. J., Kodama, T., Tanaka, H., Komoto, K., Suyama, S., Ono, T., and Yamakawa, T.: Isoscapes reveal patterns of δ13C and δ15N of pelagic forage fish and squid in the Northwest Pacific Ocean, Prog. Oceanogr., 175, 124-138, https://doi.org/10.1016/j.pocean.2019.04.003, 2019.

Ohshimo, S., Tawa, A., Ota, T., Nishimoto, S., Ishihara, T., Watai, M., Satoh, K., Tanabe, T., and Abe, O.: Horizontal distribution and habitat of Pacific bluefin tuna, *Thunnus orientalis*, larvae in the waters around Japan, Bull. Mar. Sci., 93, 769-787, https://doi.org/10.5343/bms.2016.1094, 2017.

Omori, M.: Weight and chemical composition of some important oceanic zooplankton in the North Pacific Ocean, Mar. Biol., 3, 4-10, https://doi.org/10.1007/bf00355587, 1969.

Ono, T.: Long-term trends of oxygen concentration in the waters in bank and shelves of the Southern Japan Sea, J. Oceanogr., https://doi.org/10.1007/s10872-021-00599-1, 2021.

Pu, X.-M., Sun, S., Yang, B., Zhang, G.-T., and Zhang, F.: Life history strategies of *Calanus sinicus* in the southern Yellow Sea in summer, J. Plankton Res., 26, 1059-1068, https://doi.org/10.1093/plankt/fbh101, 2004a.

Pu, X.-M., Sun, S., Yang, B., Ji, P., Zhang, Y.-S., and Zhang, F.: The combined effects of temperature and food supply on *Calanus sinicus* in the southern Yellow Sea in summer, J. Plankton Res., 26, 1049-1057, https://doi.org/10.1093/plankt/fbh097, 2004b.

Ren, H., Chen, Y. C., Wang, X. T., Wong, G. T. F., Cohen, A. L., DeCarlo, T. M., Weigand, M. A., Mii, H. S., and Sigman, D. M.: 21st-century rise in anthropogenic nitrogen deposition on a remote coral reef, Science, 356, 749-752, https://doi.org/10.1126/science.aal3869, 2017.

Smyntek, P. M., Teece, M. A., Schulz, K. L., and Thackeray, S. J.: A standard protocol for stable isotope analysis of zooplankton in aquatic food web research using mass balance correction models, Limnol. Oceanogr., 52, 2135-2146, https://doi.org/10.4319/lo.2007.52.5.2135, 2007.

Sugimoto, R., Tsuboi, T., and Fujita, M. S.: Comprehensive and quantitative assessment of nitrate dynamics in two contrasting forested basins along the Sea of Japan using dual isotopes of nitrate, Sci. Total Environ., 687, 667-678, https://doi.org/10.1016/j.scitotenv.2019.06.090, 2019.

Tanaka, H., Takasuka, A., Aoki, I., and Ohshimo, S.: Geographical variations in the trophic ecology of Japanese anchovy, *Engraulis japonicus*, inferred from carbon and nitrogen stable isotope ratios, Mar. Biol., 154, 557-568, https://doi.org/10.1007/s00227-008-0949-4, 2008.

Uye, S.: Why does *Calanus sinicus* prosper in the shelf ecosystem of the Northwest Pacific Ocean?, ICES J. Mar. Sci., 57, 1850-1855, https://doi.org/10.1006/jmsc.2000.0965, 2000.

Uye, S. and Yamamoto, F.: In situ feeding of the planktonic copepod *Calanus sinicus* in the Inland Sea examined by the gut fluorescence method, Bull. Plankton Soc. Japan, 42, 123-139, 1995.

Yi, X., Huang, Y., Zhuang, Y., Chen, H., Yang, F., Wang, W., Xu, D., Liu, G., and Zhang, H.: In situ diet of the copepod Calanus sinicus in coastal waters of the South Yellow Sea and the Bohai Sea, Acta Oceanol. Sin., 36, 68-79, https://doi.org/10.1007/s13131-017-0974-6, 2017.

Zhou, K., Sun, S., Wang, M., Wang, S., and Li, C.: Differences in the physiological processes of *Calanus sinicus* inside and outside the Yellow Sea Cold Water Mass, J. Plankton Res., 38, 551-563, https://doi.org/10.1093/plankt/fbw011, 2016.

Table 1. Numbers of samples of *Calanus sinicus* for stable isotope analysis.

Station	**March**	**April**	**May**	**June**	**Total**
TB (Toyama Bay)	4	14	20	7	45
Copepodite 5	0	5	6	0	11
Female	0	0	5	0	5
Male	0	0	2	0	2
Mixed	0	9	7	7	27
IB (Iida Bay)	5	20	9	6	40
Copepodite 5	0	3	1	0	4
Female	0	4	5	0	9
Male	0	3	1	0	4
Mixed	5	10	2	6	23
NN (Northern part of Noto)	38	60	34	12	144
Copepodite 5	9	21	11	4	45
Female	15	25	12	3	55
Male	14	14	11	5	44
Mixed	0	0	0	0	0
WB (Wakasa Bay)	14	22	1	8	45
Copepodite 5	0	2	0	0	2
Female	2	7	0	0	9
Male	5	1	0	0	6
Mixed	7	12	1	8	28
Total	**61**	**116**	**64**	**33**	**274**
Copepodite 5	9	31	18	4	62
Female	17	36	22	3	78
Male	19	18	14	5	56
Mixed	16	31	10	21	78

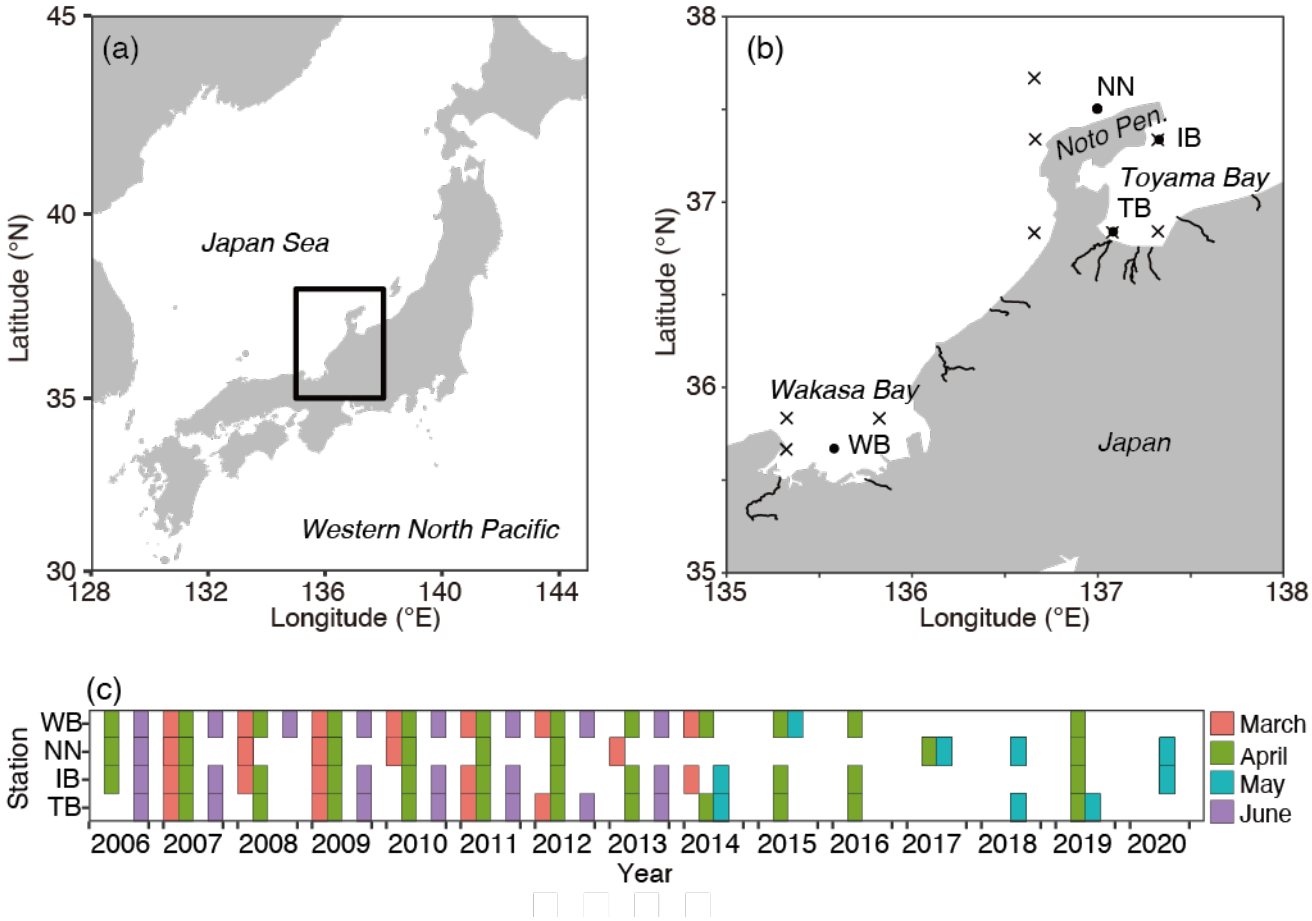

480 **Figure 1: Sampling locations and dates.** (a) Location of the study area in the Japan Sea. (b) Distribution of sampling stations of *Calanus sinicus* (closed circles) and particulate organic matter (POM) for stable isotope analysis along the Japanese coast of the Japan Sea. (c) Months and years of samplings of *C. sinicus* at the four stations. The lines in (b) denote the downstream reaches of class A rivers. The maps were made with Natural Earth, and Geospatial Information Authority of Japan.

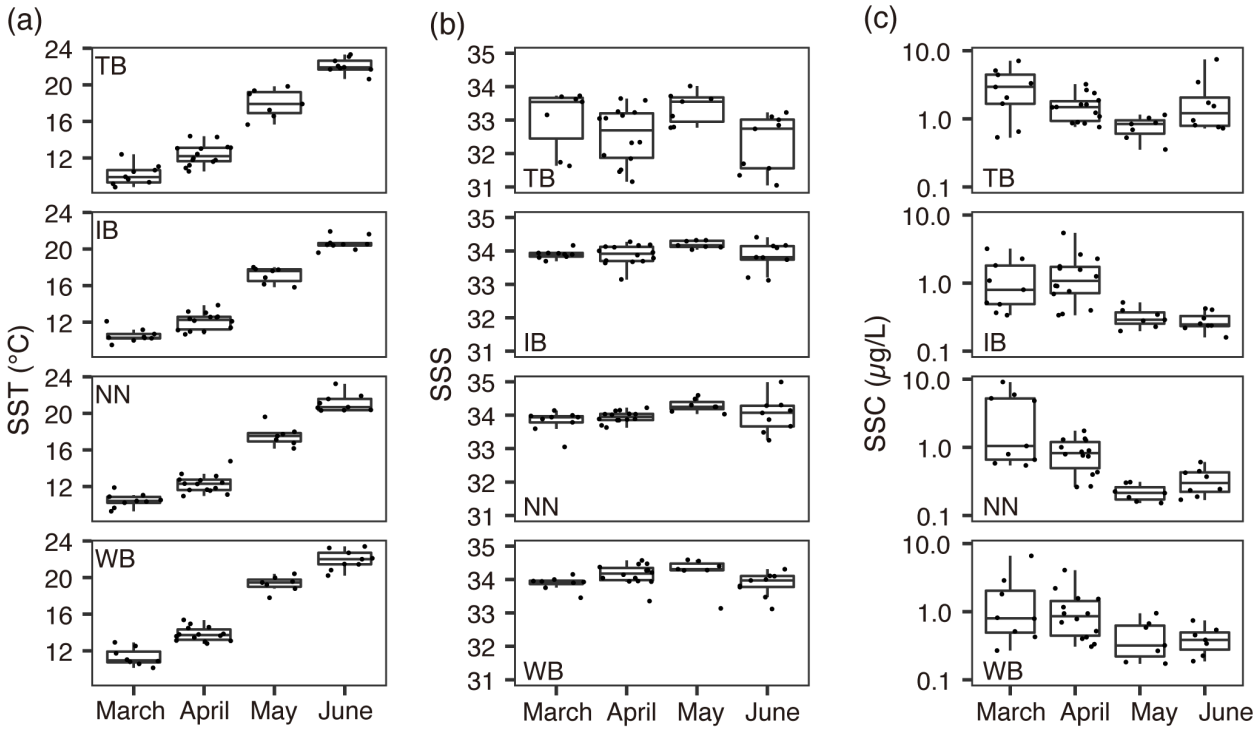

Figure 2: Variations of environmental parameters among months and stations. (a) Sea surface temperature (SST), (b) Sea surface salinity (SSS), and (c) Sea surface chlorophyll *a* concentration (SSC). Values at TB, IB, NN, and WB are shown. Boxplots show the medians (horizontal lines within boxes), upper and lower quartiles (boxes), and quartile deviations (bars). Small points are raw data points. In (b), the lowest outlier at TB in March (SSS = 28) is not shown.

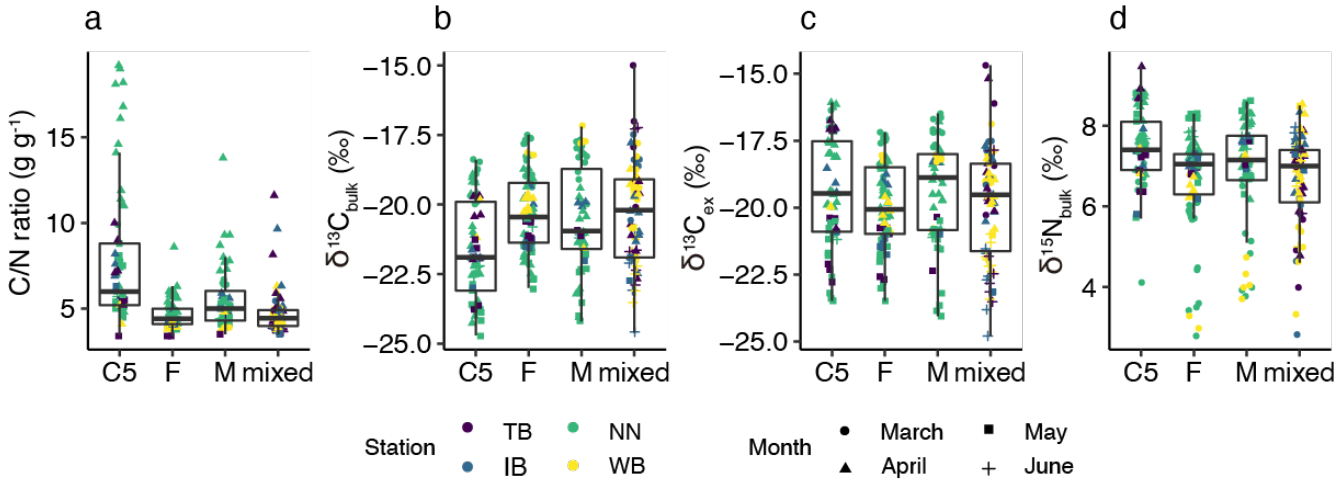

Figure 3: Variations of (a) C/N ratio, (b) $\delta^{13}C_{bulk}$, (c) $\delta^{13}C_{ex}$, and (b) $\delta^{15}N_{bulk}$ values in *C. sinicus* among growth stages and sex. The growth stages and sex of *C. sinicus* were divided into copepodite V (C5), adult female (F), adult male (M) and mixed (undivided). Boxplots show the medians (horizontal lines within boxes), upper and lower quartiles (boxes), and quartile deviations (bars). Small points are raw data points, and the colors and shapes of points indicate stations and sampling months, respectively.

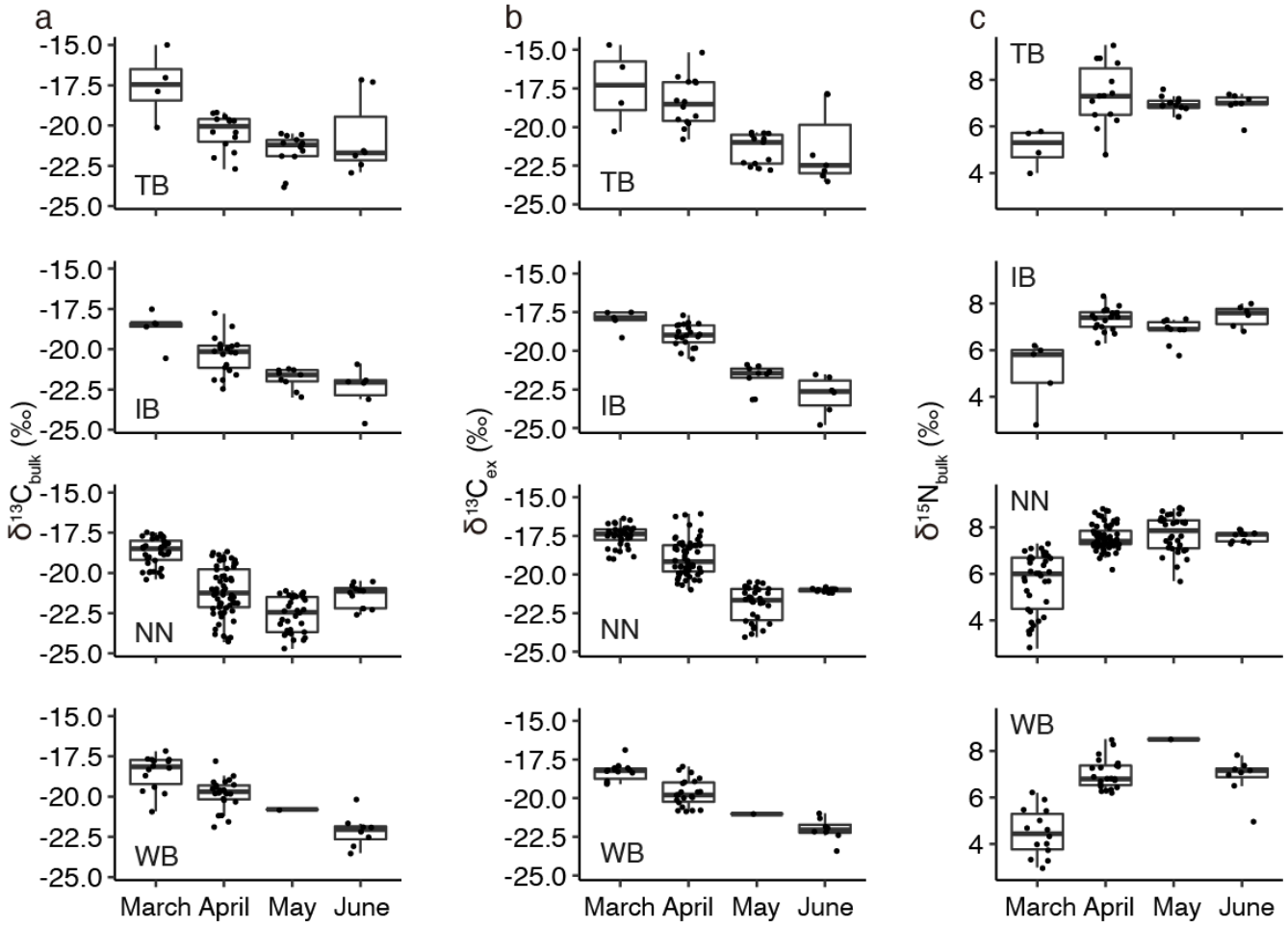

500 **Figure 4: Variations of (a) $\delta^{13}C_{bulk}$, (b) $\delta^{13}C_{ex}$, and (c) $\delta^{15}N_{bulk}$ values of *C. sinicus* among months and stations.** The variations at TB, IB, NN, and WB are shown. Boxplots show the means (horizontal lines within boxes), standard deviations (boxes), and maximum or minimum values (bars). Small points are raw data points.

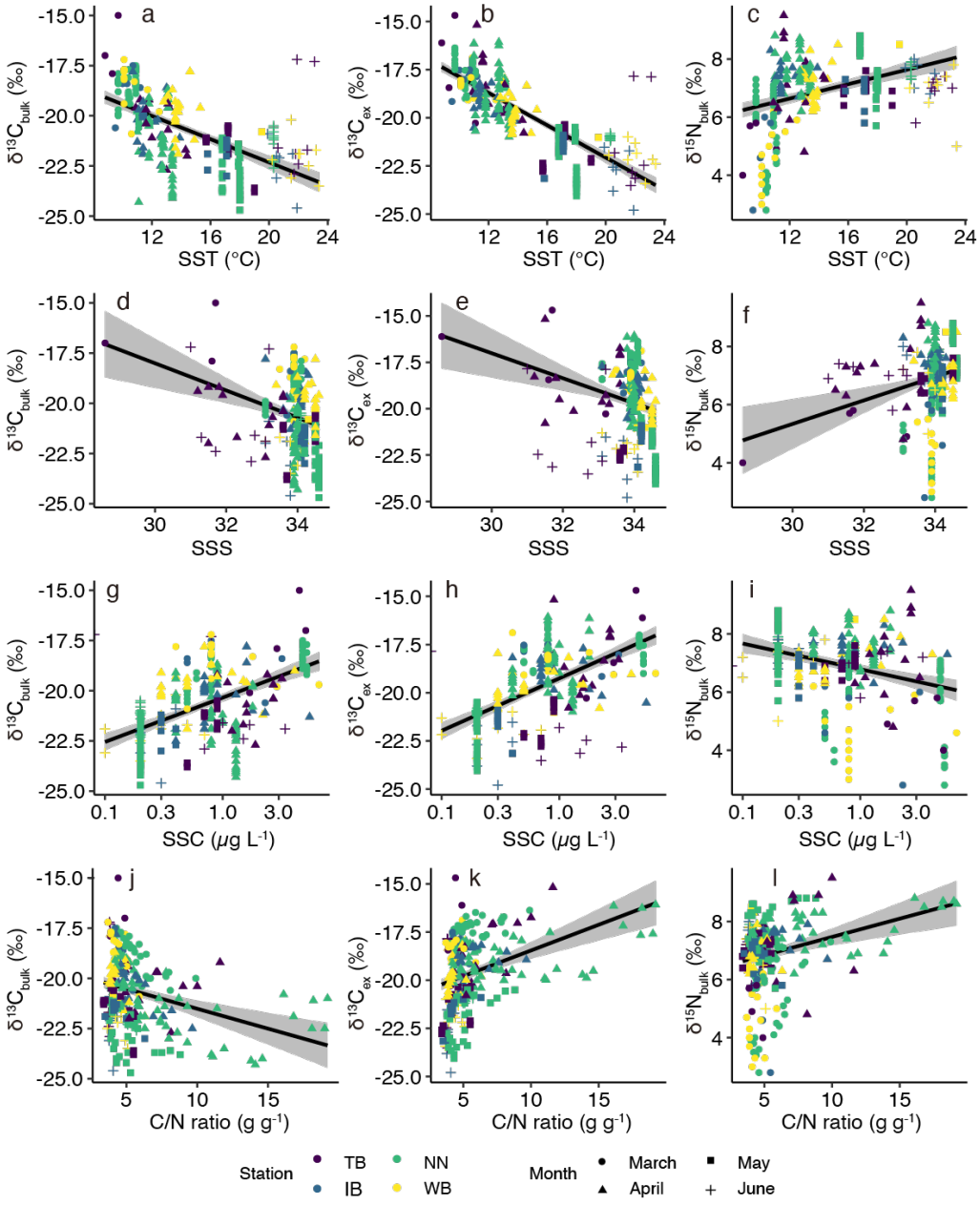

505 **Figure 5: Relationships between (a) $\delta^{13}C_{bulk}$ and sea surface temperature (SST), (b) $\delta^{13}C_{ex}$ and SST, (c) $\delta^{15}N_{bulk}$ and SST, (d) $\delta^{13}C_{bulk}$ and sea surface salinity (SSS), (e) $\delta^{13}C_{ex}$ and SSS, (f) $\delta^{15}N_{bulk}$ and SSS, (g) $\delta^{13}C_{bulk}$ and sea surface chlorophyll *a* concentration (SSC), (h) $\delta^{13}C_{ex}$ and SSC, (i) $\delta^{15}N_{bulk}$ and SSC, (j) $\delta^{13}C_{bulk}$ and carbon: nitrogen ratio (C/N ratio), (k) $\delta^{13}C_{ex}$ and C/N ratio, and (l) $\delta^{15}N_{bulk}$ and C/N ratio.** The colors and shapes of points indicate stations and sampling months, respectively. The black lines and gray shading indicate linear regression lines and 95% confidence intervals, respectively. The 510 SSC values (g–h) were transformed as logarithm values.

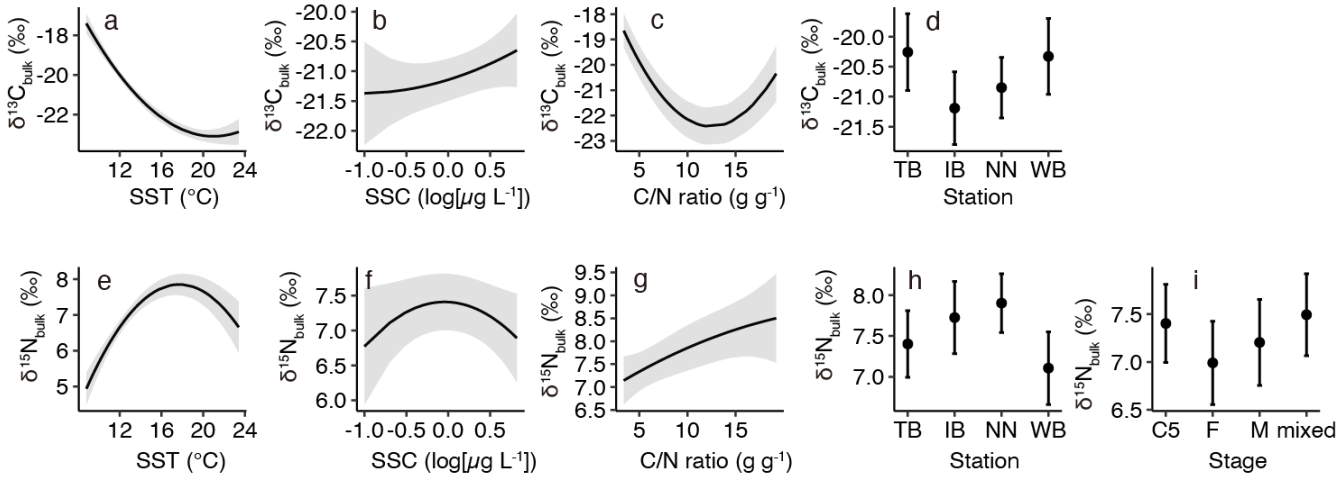

Figure 6: Responses of least-Akaike information criterion (AIC) generalized linear models (GLMs) based on least squares mean (predicted) values. (a) $\delta^{13}C_{bulk}$ versus sea surface temperature (SST), (b) $\delta^{13}C_{bulk}$ versus sea surface chlorophyll *a* concentration (SSC), (c) $\delta^{13}C_{bulk}$ versus carbon:nitrogen (C/N) ratio, (d) $\delta^{13}C_{bulk}$ versus stations, (e) $\delta^{15}N_{bulk}$ versus SST, (f) $\delta^{15}N_{bulk}$ versus SSC, and (g) $\delta^{15}N_{bulk}$ versus C/N ratio, (h) $\delta^{15}N_{bulk}$ versus station, and (i) $\delta^{15}N_{bulk}$ versus stages. Black lines with gray shading (a–c, e–g) or closed circles with vertical bars (d, h and i) denote the predicted values with 95% confidence limits based on the GLMs.

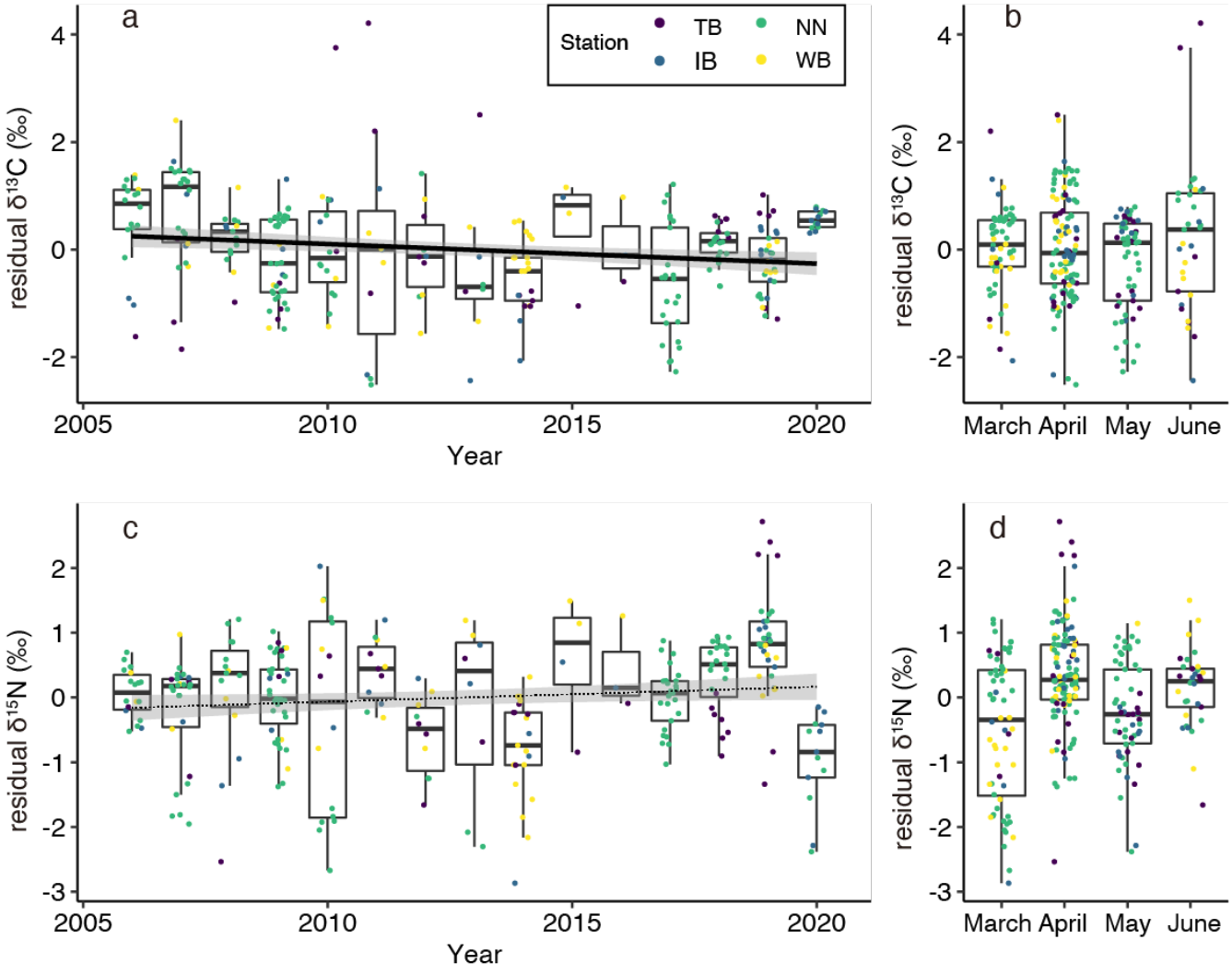

Figure 7: (a) Interannual and (b) monthly variations of residual $\delta^{13}C$ (residuals of $\delta^{13}C$ in the GLM) values and (c) interannual and (b) monthly variations of residual $\delta^{15}N$ values. Boxplots show the medians (horizontal lines within boxes), upper and lower quartiles (boxes), and quartile deviations (bars). Small points are raw data points, and the colors of points indicate stations. The black lines and gray shading (a, c) indicate linear regression lines and 95% confidence intervals, respectively. The coefficient of regression line was significantly different from 0 between residual $\delta^{13}C$ and year (solid line), but not between residual $\delta^{15}N$ and year (dotted line).